The roles of metallic rectangular-grating and planar anodes in the photocarrier generation and transport of organic solar cells—Supplementary material

Wei E.I. Sha, Wallace C.H. Choy, and Weng Cho Chew

Department of Electrical and Electronic Engineering,
the University of Hong Kong, Pokfulam Road, Hong Kong.
Email: wsha@eee.hku.hk (W.E.I. Sha)

November 3, 2012

S1 Multiphysics Modeling

S1.1 Maxwell's equations

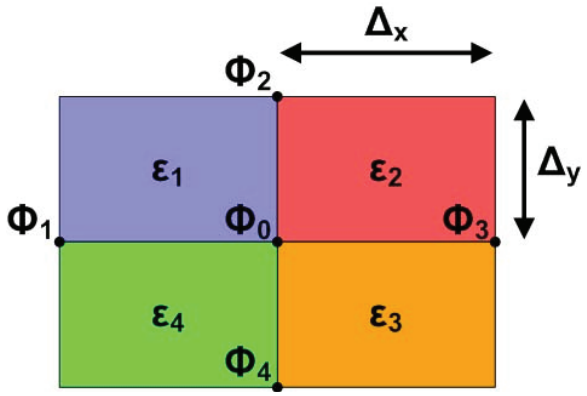

Figure S1: (Color online) The five-point stencil for the FDFD method. Δ_x and Δ_y are respectively the spatial steps along the x and y directions. $\Phi = E_z$ for the TE polarization and $\Phi = H_z$ for the TM polarization. Here, $\epsilon = n_c^2$ is the relative permittivity in the discretized region and n_c is the complex refractive index of the optical material.

Considering a two-dimensional organic solar cell (OSC) structure, the Maxwell's equations can be decoupled into a TE and TM modes. The wave equations

for TE and TM modes are respectively formulated as

$$\frac{1}{\epsilon_r}\frac{\partial}{\partial x}\left(\frac{1}{\mu_r}\frac{\partial E_z}{\partial x}\right)+\frac{1}{\epsilon_r}\frac{\partial}{\partial y}\left(\frac{1}{\mu_r}\frac{\partial E_z}{\partial y}\right)+k_0^2E_z=0 \tag{S1}$$

$$\frac{1}{\mu_r}\frac{\partial}{\partial x}\left(\frac{1}{\epsilon_r}\frac{\partial H_z}{\partial x}\right)+\frac{1}{\mu_r}\frac{\partial}{\partial y}\left(\frac{1}{\epsilon_r}\frac{\partial H_z}{\partial y}\right)+k_0^2H_z=0 \tag{S2}$$

where k_0 is the wave number of incident light, and ϵ_r and μ_r are the relative permittivities and permeabilities, respectively. Regarding non-magnetic optical materials, $\mu_r=1$, $\epsilon_r=n_c^2$, and n_c is the complex refractive index of optical materials.

With the Yee lattice, the 2D finite-difference frequency-domain (FDFD) method is utilized to characterize the optical properties of OSCs. As shown in Fig. S1, the five-point stencil is adopted for the FDFD method. The discretized forms for the TE and TM wave equations are respectively of the form

$$2\left(\frac{1}{\Delta_x^2}+\frac{1}{\Delta_y^2}\right)\frac{\Phi_0}{\bar{\epsilon}}-k_0^2\Phi_0-\frac{\Phi_1+\Phi_3}{\bar{\epsilon}\Delta_x^2}-\frac{\Phi_2+\Phi_4}{\bar{\epsilon}\Delta_y^2}=0,\quad \Phi=E_z \tag{S3}$$

$$\begin{aligned}2\left(\frac{1}{\Delta_x^2}+\frac{1}{\Delta_y^2}\right)\frac{\Phi_0}{\bar{\epsilon}}-k_0^2\Phi_0-\frac{\epsilon_1^{-1}+\epsilon_4^{-1}}{2\Delta_x^2}\Phi_1-\frac{\epsilon_2^{-1}+\epsilon_3^{-1}}{2\Delta_x^2}\Phi_3\\ -\frac{\epsilon_1^{-1}+\epsilon_2^{-1}}{2\Delta_y^2}\Phi_2-\frac{\epsilon_3^{-1}+\epsilon_4^{-1}}{2\Delta_y^2}\Phi_4=0,\quad \Phi=H_z\end{aligned} \tag{S4}$$

$$\bar{\epsilon}=\begin{cases}\dfrac{\epsilon_1+\epsilon_2+\epsilon_3+\epsilon_4}{4}, & \Phi=E_z\\ 4(\epsilon_1^{-1}+\epsilon_2^{-1}+\epsilon_3^{-1}+\epsilon_4^{-1})^{-1}, & \Phi=H_z\end{cases} \tag{S5}$$

Although Eqs. (S3) and (S4) can in principle treat the dielectric-dielectric and dielectric-metal interfaces, they will lose some accuracy at the interfaces and cannot well reproduce the features of exponentially decayed surface plasmon waves. Thus a one-sided difference scheme is developed to rectify the problem. For the horizontal interface ($y=y_h$) between the media 1 and 2, the flexible and high-order-accurate one-sided difference reads

$$\begin{aligned}\frac{\partial}{\partial y}\Phi^1\Big|_{x=i\Delta_x}&\approx\frac{1.5\Phi^1(i,j)-2\Phi^1(i,j-1)+0.5\Phi^1(i,j-2)}{\Delta_y}\\ \frac{\partial}{\partial y}\Phi^2\Big|_{x=i\Delta_x}&\approx\frac{-1.5\Phi^2(i,j)+2\Phi^2(i,j+1)-0.5\Phi^2(i,j+2)}{\Delta_y}\end{aligned} \tag{S6}$$

For the vertical interfaces, one can also use the scheme.

The incident Sunlight reflected by OSC devices converts to outgoing waves propagating into infinite air (or free-space) region. A perfectly matched

layer (PML) absorbs the outgoing waves without spurious reflections and "perfectly" simulates unbounded wave propagations. The wave equation with the complex coordinate stretched PML is given by

$$\frac{1}{s_r(x)}\frac{\partial}{\partial x}\left(\frac{1}{s_r(x)}\frac{\partial \Phi}{\partial x}\right)+\frac{1}{s_r(y)}\frac{\partial}{\partial y}\left(\frac{1}{s_r(y)}\frac{\partial \Phi}{\partial y}\right)+k_0^2\Phi=0 \tag{S7}$$

where $s_r = 1 + i_0\sigma/\omega\epsilon_0$, i_0 is the imaginary unit, ϵ_0 is the permittivity of free-space, and the conductivities $\sigma(x)$ and $\sigma(y)$ are non-zeros only within PML layers normal to the x- and y-axes, respectively. The optimized conductivities are chosen as,

$$\begin{aligned}\sigma_i &= \frac{0.02}{\Delta}\left(\frac{2i-1}{16}\right)^{3.7}, \quad i=1,...,8\\ \sigma_{i+0.5} &= \frac{0.02}{\Delta}\left(\frac{2i}{16}\right)^{3.7}, \quad i=0,...,8\end{aligned} \tag{S8}$$

where $\Delta = \Delta_x$ or $\Delta = \Delta_y$ for the PML layers normal to the x- or y-axis, and i is the grid index of the eight-layer PML.

At the outermost boundary of the PML, a Mur ABC replacing the traditional perfectly electric conductor truncation boundary is employed to further reduce the spurious numerical reflections. Taking the top plane $y = 0$ as an example, the second-order Mur ABC can be written as

$$\left[\frac{\partial}{\partial y}+i_0\left(k_0+\frac{1}{2k_0}\frac{\partial^2}{\partial x^2}\right)\right]\Phi\Big|_{y=0}=0 \tag{S9}$$

and its discretized form is

$$f_1\Phi(i,j)+f_2\Phi(i-1,j)+f_3\Phi(i+1,j)+f_4\Phi(i,j+1)=0 \tag{S10}$$

where

$$\begin{aligned}f_1 &= 2\exp(-i_0k_0\Delta_y)-2k_0^2\Delta_x^2\exp(-i_0k_0\Delta_y)-2\\ f_2 &= f_3 = 1-\exp(-i_0k_0\Delta_y)\\ f_4 &= 2k_0^2\Delta_x^2\end{aligned} \tag{S11}$$

Regarding a periodic OSC device, the periodic boundary conditions need to be implemented. According to the Floquet or Bloch theorem, we have

$$\begin{aligned}\Phi(x+P,y) &= \Phi(x,y)\exp\left(i_0k_0\sin\theta\cdot P\right)\\ \Phi(x,y) &= \Phi(x+P,y)\exp\left(-i_0k_0\sin\theta\cdot P\right)\end{aligned} \tag{S12}$$

where P is the periodicity and θ is the incident angle with respect to the y axis.

It should be noted that the FDFD equations of (S1) and (S2) are specially for total field. The scattered field equations to be solved can be derived by using the relations

$$H_z = H_z^i + H_z^s \tag{S13}$$

and

$$E_z = E_z^i + E_z^s \tag{S14}$$

where E_z^i (H_z^i) is the incident electric-field (magnetic-field), and E_z^s (H_z^s) is the scattered electric-field (magnetic-field).

S1.2 Extraction of exciton generation rate

The exciton generation rate can be written as

$$G(\mathbf{r}) = \int_{400\,\mathrm{nm}}^{800\,\mathrm{nm}} \frac{2\pi}{h} n_r(\lambda) k_i(\lambda) \epsilon_0 |\mathbf{E}(\mathbf{r}, \lambda)|^2 \Gamma(\lambda) d\lambda \tag{S15}$$

where h is the Planck constant, $n_c = n_r + ik_i$ is the complex refractive index of the active polymer material, $\mathbf{E}$ is the (optical) electric field that can be obtained by solving the Maxwell's equations, and Γ is the solar irradiance spectrum of AM 1.5G. Moreover, the exciton generation rate is the average value of those for TE and TM polarizations.

S1.3 Semiconductor equations

For studying electrical properties of OSCs, one should self-consistently solve the coupled nonlinear semiconductor equations (Poisson, continuity, and drift-diffusion equations) given by

$$\nabla \cdot (\epsilon^d \nabla \phi) = -q(p - n) \tag{S16}$$

$$\frac{\partial n}{\partial t} = \frac{1}{q} \nabla \cdot (-q\mu_n n \nabla \phi + q D_n \nabla n) + QG - (1 - Q)R \tag{S17}$$

$$\frac{\partial p}{\partial t} = \frac{-1}{q} \nabla \cdot (-q\mu_p p \nabla \phi - q D_p \nabla p) + QG - (1 - Q)R \tag{S18}$$

In the above, ϵ^d is the dielectric constant of the polymer active material, q is the electron charge, ϕ is the electrical potential, and n (p) is the electron (hole) concentration. Moreover, μ_n (μ_p) is the electron (hole) mobility, and D_n (D_p) is the electron (hole) diffusion coefficient accessible by Einstein relations and mobilities. Furthermore, $\mathbf{J}_n = -q\mu_n n \nabla \phi + q D_n \nabla n$ and $\mathbf{J}_p = -q\mu_p p \nabla \phi - q D_p \nabla p$ are respectively electron and hole current densities, and G is the exciton generation rate of Eq. (S15) obtained with Maxwell's equations. In addition, R is the bimolecular recombination rate and Q is the field and temperature dependent exciton dissociation probability, which is a unique parameter for OSCs.

The theory of geminate recombination proposed that the probability of exciton dissociation is distance, field, and temperature dependent

$$p(x,F,T) = \frac{k_d(x,F,T)}{k_d(x,F,T)+k_r} \tag{S19}$$

where F is the internal E-field, x is the distance between the bounded charges of the exciton, k_r is the rate at which excitons relax to the ground state, and k_d is the dissociation rate

$$k_d(x,F,T) = \frac{3\gamma}{4\pi x^3} e^{-U_b/(k_B T)} \frac{J_1(2\sqrt{-2b})}{\sqrt{-2b}} \tag{S20}$$

where $U_b = \frac{q^2}{4\pi\epsilon_r\epsilon_0 x}$ is the exciton binding energy, J_1 is the first order Bessel function, and the field parameter $b = \frac{q^3 F}{8\pi\epsilon_0\epsilon_r k_B^2 T^2}$.

In disordered polymer systems, it is appropriate to treat the charge-separation distance not as a constant, but instead as a distribution of distances. A spherically averaged Gaussian distribution has been shown to be most appropriate, for which the overall exciton dissociation probability becomes an integral over all charge-separation distances. The exciton dissociation probability Q is finally given by

$$Q(F,T) = \frac{4}{\sqrt{\pi}a^3} \int_0^\infty p(x,F,T) x^2 \exp\left[-\left(\frac{x}{a}\right)^2\right] dx \tag{S21}$$

where a is the averaged electron-hole pair distance.

Using the Scharfetter-Gummel scheme in the spatial domain and using the semi-implicit strategy in the temporal domain, the 2D discretized forms of Eqs. (S16), (S17), and (S18) are respectively given by

$$\begin{aligned}
&\frac{1}{\Delta_x^2}\epsilon^d_{i+1/2,j}\phi^{t+1}_{i+1,j} + \frac{1}{\Delta_x^2}\epsilon^d_{i-1/2,j}\phi^{t+1}_{i-1,j} + \frac{1}{\Delta_y^2}\epsilon^d_{i,j+1/2}\phi^{t+1}_{i,j+1} + \frac{1}{\Delta_y^2}\epsilon^d_{i,j-1/2}\phi^{t+1}_{i,j-1} \\
&- \left(\epsilon^d_{i+1/2,j} + \epsilon^d_{i-1/2,j} + \epsilon^d_{i,j+1/2} + \epsilon^d_{i,j-1/2}\right)\left(\frac{1}{2\Delta_x^2} + \frac{1}{2\Delta_y^2}\right)\phi^{t+1}_{i,j} - \frac{n^t_{i,j} + p^t_{i,j}}{U_t}\phi^{t+1}_{i,j} \\
&= q(n^t_{i,j} - p^t_{i,j}) - \frac{n^t_{i,j} + p^t_{i,j}}{U_t}\phi^t_{i,j}
\end{aligned} \tag{S22}$$

$$\frac{n_{i,j}^{t+1}-n_{i,j}^{t}}{\Delta_t}=Q_{i,j}^{t}G_{i,j}-(1-Q_{i,j}^{t})R_{i,j}^{t}+\frac{D_{i+1/2,j}^{n}}{\Delta_x^2}B\left(\frac{\phi_{i+1,j}^{t+1}-\phi_{i,j}^{t+1}}{U_t}\right)n_{i+1,j}^{t+1}$$
$$+\frac{D_{i-1/2,j}^{n}}{\Delta_x^2}B\left(\frac{\phi_{i-1,j}^{t+1}-\phi_{i,j}^{t+1}}{U_t}\right)n_{i-1,j}^{t+1}+\frac{D_{i,j+1/2}^{n}}{\Delta_y^2}B\left(\frac{\phi_{i,j+1}^{t+1}-\phi_{i,j}^{t+1}}{U_t}\right)n_{i,j+1}^{t+1}$$
$$+\frac{D_{i,j-1/2}^{n}}{\Delta_y^2}B\left(\frac{\phi_{i,j-1}^{t+1}-\phi_{i,j}^{t+1}}{U_t}\right)n_{i,j-1}^{t+1}-\left[\frac{D_{i+1/2,j}^{n}}{\Delta_x^2}B\left(\frac{\phi_{i,j}^{t+1}-\phi_{i+1,j}^{t+1}}{U_t}\right)\right.$$
$$+\frac{D_{i-1/2,j}^{n}}{\Delta_x^2}B\left(\frac{\phi_{i,j}^{t+1}-\phi_{i-1,j}^{t+1}}{U_t}\right)+\frac{D_{i,j+1/2}^{n}}{\Delta_y^2}B\left(\frac{\phi_{i,j}^{t+1}-\phi_{i,j+1}^{t+1}}{U_t}\right)$$
$$\left.+\frac{D_{i,j-1/2}^{n}}{\Delta_y^2}B\left(\frac{\phi_{i,j}^{t+1}-\phi_{i,j-1}^{t+1}}{U_t}\right)\right]n_{i,j}^{t+1} \tag{S23}$$

$$\frac{p_{i,j}^{t+1}-p_{i,j}^{t}}{\Delta_t}=Q_{i,j}^{t}G_{i,j}-(1-Q_{i,j}^{t})R_{i,j}^{t}+\frac{D_{i+1/2,j}^{p}}{\Delta_x^2}B\left(\frac{\phi_{i,j}^{t+1}-\phi_{i+1,j}^{t+1}}{U_t}\right)p_{i+1,j}^{t+1}$$
$$+\frac{D_{i-1/2,j}^{p}}{\Delta_x^2}B\left(\frac{\phi_{i,j}^{t+1}-\phi_{i-1,j}^{t+1}}{U_t}\right)p_{i-1,j}^{t+1}+\frac{D_{i,j+1/2}^{p}}{\Delta_y^2}B\left(\frac{\phi_{i,j}^{t+1}-\phi_{i,j+1}^{t+1}}{U_t}\right)p_{i,j+1}^{t+1}$$
$$+\frac{D_{i,j-1/2}^{p}}{\Delta_y^2}B\left(\frac{\phi_{i,j}^{t+1}-\phi_{i,j-1}^{t+1}}{U_t}\right)p_{i,j-1}^{t+1}-\left[\frac{D_{i+1/2,j}^{p}}{\Delta_x^2}B\left(\frac{\phi_{i+1,j}^{t+1}-\phi_{i,j}^{t+1}}{U_t}\right)\right.$$
$$+\frac{D_{i-1/2,j}^{p}}{\Delta_x^2}B\left(\frac{\phi_{i-1,j}^{t+1}-\phi_{i,j}^{t+1}}{U_t}\right)+\frac{D_{i,j+1/2}^{p}}{\Delta_y^2}B\left(\frac{\phi_{i,j+1}^{t+1}-\phi_{i,j}^{t+1}}{U_t}\right)$$
$$\left.+\frac{D_{i,j-1/2}^{p}}{\Delta_y^2}B\left(\frac{\phi_{i,j-1}^{t+1}-\phi_{i,j}^{t+1}}{U_t}\right)\right]p_{i,j}^{t+1} \tag{S24}$$

where $B(x)=\frac{x}{e^x-1}$ is the Bernoulli function and $U_t=\frac{k_BT}{q}$. It should be noted that the Gummel's method has been incorporated in (S22) to accelerate the convergence of the nonlinear semiconductor equations. Since the dependent variables (ϕ, n, p) in the basic equations are of greatly different orders of magnitude and show a strongly different behaviors in regions with small and large space charge, the scaling procedure must be executed to guarantee the numerical stability of the algorithm. Here, we redefine 5 independent basic units as listed in Table SI. Meanwhile, we keep the mathematical forms of nonlinear semiconductor equations unchanged.

The boundary conditions play a key role in modeling electrical properties of plasmonic OSCs. The potential boundary condition for the Schottky

Table SI: Scaled independent basic units. $\max\{\text{DOS}\}$ denotes maximum effective density of states (cm^{-3}).

cm	$\max\{\text{DOS}\}^{1/3}$
s	10^{12}
V	1
C	$\frac{1}{1.602\times10^{-19}}$
K	$\frac{1}{300}$

contact is given by

$$\phi = V_a - \frac{W_m}{q} \tag{S25}$$

where V_a is the applied voltage, and W_m is the metal work function. For the ohmic contact, the built-in potential is the potential difference between the highest occupied molecular orbital (HOMO) of donor and lowest unoccupied molecular orbital (LUMO) of acceptor. The Neumann (floating) boundary condition is used to truncate the left and right boundaries of OSCs, i.e.

$$\frac{\partial \phi}{\partial N} = 0,\ \frac{\partial n}{\partial N} = 0,\ \frac{\partial p}{\partial N} = 0 \tag{S26}$$

where N are the normal vectors of the left and right boundaries of OSCs. The boundary conditions for the top and bottom electrodes can be written as

$$n = N_c \exp\left(-\frac{\psi_b^n}{k_B T}\right),\ \text{for cathode} \tag{S27}$$

$$p = N_v \exp\left(-\frac{\psi_b^p}{k_B T}\right),\ \text{for anode} \tag{S28}$$

where N_c and N_v are the effective state density of electrons and holes, respectively. ψ_b^n is the injection barrier between the LUMO and the cathode, and ψ_b^p is the injection barrier between the HOMO and the anode. It should be noted that the infinite surface recombination velocity is assumed for the Schottky contact.

S1.4 Discretization criteria

The spatial steps of Maxwell's equations and semiconductor equations depend on the material wavelength and carrier Debye length, respectively. Regarding typical OSCs, we use the uniform grid to discretize Maxwell's equations and semiconductor equations with a spatial step of 1 nm. The time step of semiconductor equations can be evaluated by

$$\Delta_t < \min\left(\frac{C\epsilon^d}{\mu_n \cdot n + \mu_p \cdot p}\right) \tag{S29}$$

Table SII: The simulation parameters for the electrical modeling of OSCs. Here, E_g is the effective band gap of the blend active material, ϵ_0 is the permittivity of free space, a is the averaged electron-hole pair distance, and k_r is the exciton decay rate.

E_g	$1.2\ eV$
μ_n	$7.4 \times 10^{-7}\ m^2/(V \cdot S)$
μ_p	$7.4 \times 10^{-8}\ m^2/(V \cdot S)$
N_c	$2.5 \times 10^{19}\ cm^{-3}$
N_v	$2.5 \times 10^{19}\ cm^{-3}$
ϵ^d	$3.4\epsilon_0\ F/m$
a	$1.12\ nm$
k_r	$3 \times 10^5\ s^{-1}$
ψ_b^n	$0.2\ eV$
ψ_b^p	$0\ eV$

where C is a tunable constant. For OSCs, $C \approx 100$ from our numerical results. Regarding both Maxwell's equations and semiconductor equations, the FD method will generate sparse matrices, which can be rapidly and efficiently inverted by the multifrontal algorithm.

S2 Simulation Parameters

Figure S2 shows the complex refractive index of the active polymer material for the optical modeling of OSCs. The complex refractive indexes of the polymer and TiO_2 are measured from ellipsometry [1]. The complex refractive index of Ag can be expressed as the Brendel-Bormann model [2]. In modeling the light absorption of OSCs, the Sun irradiance spectrum of AM 1.5G is adopted. Table SII lists the simulation parameters for the electrical modeling of OSCs.

S3 Results of Exciton Generation Rates

Figures S3 and S4 are the exciton generation rates by Eq. (S15) for the standard and plasmonic OSCs, respectively.

S4 Electrical Results at Maximum Power Point

Fig. S5 and Fig. S6 show the potential distribution, recombination rate, electron and hole current densities at the maximum power point for the standard and plasmonic OSCs, respectively.

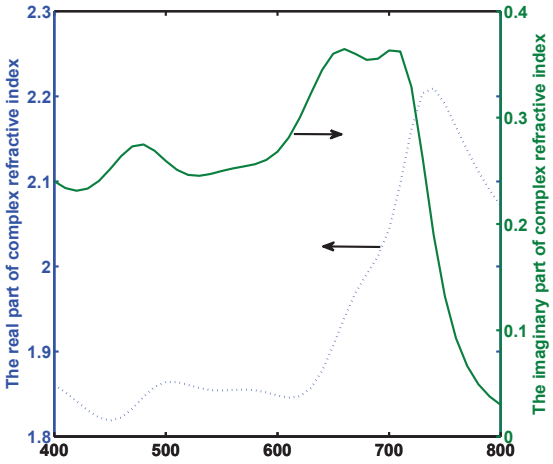

Figure S2: (Color online) The complex refractive index of the active polymer material. The active material is PBDTTT-C-T (poly{[4,8-bis-(2-ethyl-hexyl-thiophene-5-yl)-benzo[1,2-b:4,5-b']dithiophene-2,6-diyl]-alt-[2-(2'-ethyl-hexanoyl)-thieno[3,4-b]thiophen-4,6-diyl]}) and $PC_{70}BM$ ([6,6]-phenyl C71-butyric acid methyl ester) as donor and acceptor, respectively. (1:1.5, weight ratio in blend polymer.)

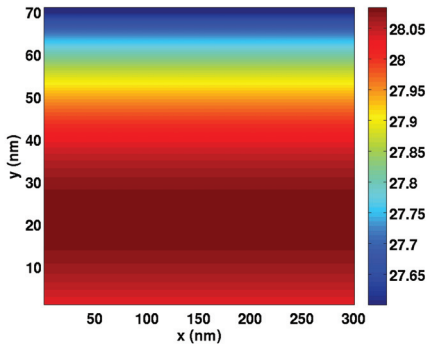

Figure S3: (Color online) The exciton generation rate of the standard OSC in the active layer.

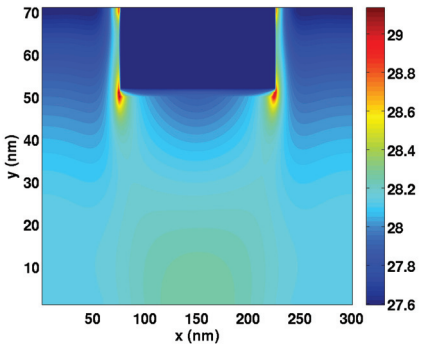

Figure S4: (Color online) The exciton generation rate of the plasmonic OSC in the active layer.

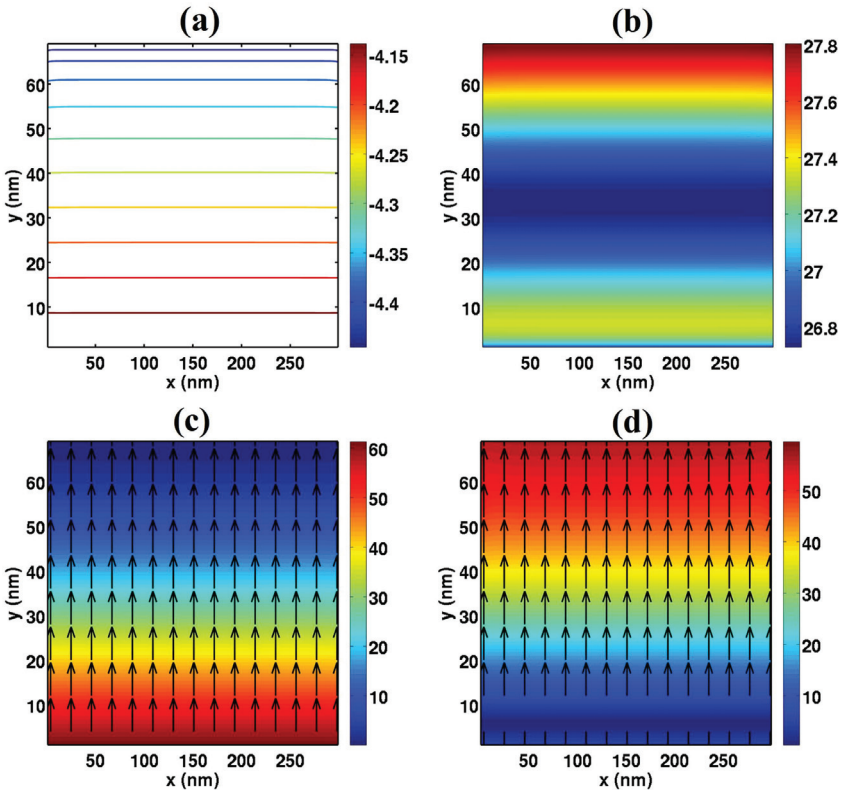

Figure S5: (Color online) The electrical results of the standard OSC at the maximum power point. (a) equipotential lines (V); (b) recombination rate with the logarithmic scale ($m^{-3}s^{-1}$); (c,d) electron and hole current densities (A/m^2). The color and arrow denote the amplitude and direction of the currents.

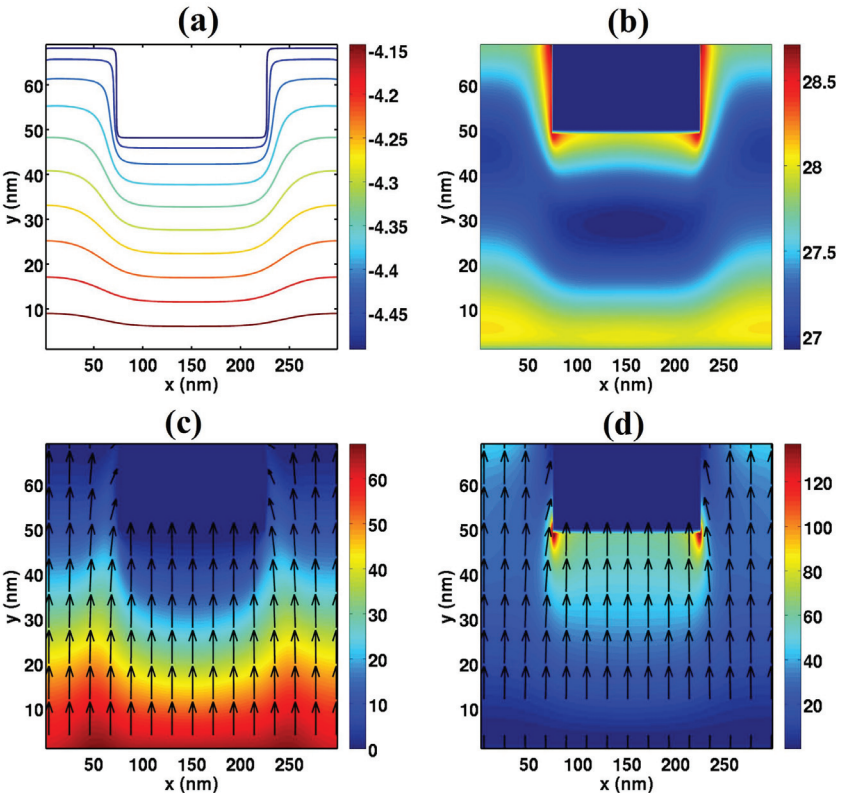

Figure S6: (Color online) The electrical results of the plasmonic OSC at the maximum power point. (a) equipotential lines (V); (b) recombination rate with the logarithmic scale ($m^{-3}s^{-1}$); (c,d) electron and hole current densities (A/m^2). The color and arrow denote the amplitude and direction of the currents.

References

[1] W. C. H. Choy and H. H. Fong, J. Phys. D: Appl. Phys. **41**, 155109 (2008).

[2] A. D. Rakic, A. B. Djurisic, J. M. Elazar, and M. L. Majewski, Appl. Optics **37**, 5271 (1998).